

000 001 002 003 004 005 006 007 008 009 010 011 012 013 014 015 016 017 018 019 020 021 022 023 024 025 026 027 028 029 030 031 032 033 034 035 036 037 038 039 040 041 042 043 044 045 046 047 048 049 050 051 052 053 CAT-PO: CROSS-MODAL ADAPTIVE TOKEN-REWARDS FOR PREFERENCE OPTIMIZATION IN TRUTHFUL MUL- TIMODAL LLMs

Anonymous authors

Paper under double-blind review

ABSTRACT

Multi-modal Large Language Models (MLLMs) have shown remarkable generative capabilities across multi-modal tasks, yet remain plagued by hallucinations where generated textual contents are semantically inconsistent with the input images. This work reveals that existing multi-modal preference optimization methods exhibit shortcomings at the preference data decoding stage. Specifically, different response tokens exhibit varying degrees of association with visual content, and consequently, their contributions to reducing hallucinations and generating high-quality responses differ. Nevertheless, most existing methods do not distinguish in their treatment, often handling them uniformly. To address this challenge, we propose a novel preference alignment method: Cross-modal Adaptive Token-rewarded Preference Optimization (Cat-PO). Building upon direct preference optimization, Cat-PO calculates hierarchical visual relevance rewards for each response token at global, local, and semantic levels. It then organically integrates these three rewards to construct a smooth reward mechanism and designs an innovative KL-based customized loss for rewarded tokens, thereby enabling fine-grained correction of hallucinatory outputs. Extensive experiments on various base models and evaluation benchmarks demonstrate that our Cat-PO can significantly reduce hallucinations and align with human preferences to enhance the truthfulness of MLLMs.

1 INTRODUCTION

The success of Multimodal Large Language Models (MLLMs) marks a significant advancement in artificial intelligence research Liu et al. (2024b); Amirloo et al. (2024). By integrating visual information with Large Language Models (LLMs), MLLMs have demonstrated unprecedented capabilities in multimodal understanding, reasoning, and interaction Xiao et al. (2024); Pi et al. (2024); Zhang et al. (2024). However, MLLMs exhibit a notable hallucination problem, where the generated textual descriptions are inconsistent with the input visual content. This phenomenon includes describing non-existent objects, incorrect object attributes, or relationships Bai et al. (2024); Gunjal et al. (2024). The hallucination issue causes a disconnect between outputs and visual facts, severely degrading user experience and undermining the reliability of downstream applications, thereby limiting their deployment in real-world scenarios Liu et al. (2024a); Liang et al. (2024).

To alleviate this issue, strategies incorporating preference learning, such as Reinforcement Learning from Human Feedback (RLHF) Christiano et al. (2017), have been widely investigated as a form of fine-tuning. The core idea is to leverage preference feedback to align model outputs with desired expectations. Recently, Direct Preference Optimization (DPO) Rafailov et al. (2023) has gained prominence for achieving excellent results without a separate reward model by simplifying complex reinforcement learning steps. Existing work demonstrates that DPO, by efficiently incorporating preference data, mitigates hallucinations in MLLMs, and improves the alignment with humans Li et al. (2023b); Zhu et al. (2024); Chen et al. (2024). However, in current human preference alignment processes, different response tokens processed by the model have varying degrees of relevance to the visual content, and their contributions to reducing hallucinations and generating high-quality answers also differ. As shown in Fig. 1 (a), When MLLMs process different tokens, the cross-modal attention they allocate to the image varies, and the token–image similarity also differs, indicating that different tokens exhibit distinct degrees of association with the visual content. Nevertheless,

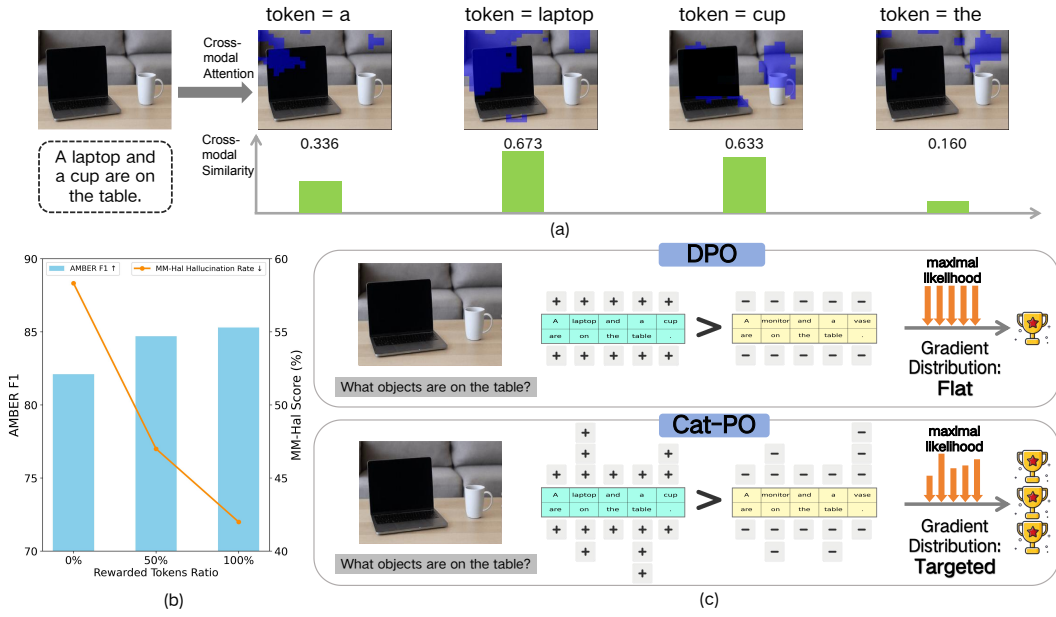


Figure 1: The motivation of our framework. (a) A visual question answering example where the model identifies "a laptop and a cup" on a table, with cross-modal attention heatmaps and cross-modal similarity scores indicating the model's visual focus and word importance in the response. (b) A performance comparison of token-rewarded DPO, showing *AMBER F1* (\uparrow) improving and *MM-Hal* Hallucination Rate (\downarrow) declining as the percentage of rewarded tokens increases. (c) A comparison of standard DPO versus our Cross-modal Adaptive Token-rewarded Preference Optimization (Cat-PO). The former uses a flat gradient distribution for maximal likelihood optimization. And the latter employs a targeted gradient distribution, suggesting potentially superior performance for the latter in refining a pre-trained MLLM.

most existing works suffer from two primary limitations: (1) They overlook the varying degrees of association between different tokens in the response and the visual content, as well as their differing contributions to high-quality outputs, treating all tokens uniformly and thus lacking fine-grained correction, as depicted in the upper part of Fig. 1 (c). (2) They rely on external visual detection models, additional noise injection techniques, expensive closed-source LLM API, or even external tools, thereby neglecting the intrinsic capabilities of MLLMs and leading to a waste of existing resources and increased costs.

Therefore, how to deeply exploit token-level fine-grained alignment signals, construct a more refined DPO feedback mechanism, and fully leverage the inherent multimodal capabilities of MLLMs to reduce additional costs and overhead remains a critical issue. Motivated by this, we conducted a series of explorations. As shown by the statistical experiment in Fig. 1 (b), when we applied DPO only to the top 50% rewarded tokens in chosen responses, we observed significant improvements in hallucination metrics AMBER-F1 and MM-Hal compared to the original DPO. Furthermore, applying DPO with all rewarded tokens yielded even more outstanding results.

Building upon these explorations, we propose a Cross-modal Adaptive Token-rewarded Preference Optimization (Cat-PO). This framework fully leverages the multimodal capabilities and advantages of MLLMs to deeply mine token-level fine-grained alignment signals between text and images, using token-rewards for Cat-PO, with the aim of more effectively mitigating hallucinations. A simplified pipeline is shown in the lower part of Fig. 1 (c). Specifically, within the MLLMs, before the image features (projected by CLIP Radford et al. (2021) and ViT) are fed into the LLM's transformer layers, we first calculate the cross-modal semantic similarity between response tokens and the image, representing the semantic relevance of tokens to visual content. Subsequently, within the transformer layers, based on the cross-modal attention of response tokens to the image, we compute the global and local relevance of each token to the visual content. Furthermore, we normalize and aggregate the three hierarchical relevance scores, map the result through an activation function, and compute the

108 final reward for each token. Finally, we design a novel Cat-PO loss based on token-level rewards
 109 and KL divergence for further optimization. Experiments on open-source datasets and benchmarks
 110 demonstrate that our Cat-PO achieves excellent performance, significantly reducing hallucinations
 111 and improving response accuracy, thereby enhancing model truthfulness. Concurrently, this work
 112 offers a new perspective on mitigating hallucinations by fully exploiting the inherent multimodal
 113 capabilities of MLLMs without introducing external technologies or tools.

114 Our main contributions are summarized as follows:
 115

- 116 1. We propose a Cross-modal Adaptive Token-rewards for Preference Optimization (Cat-PO) in
 117 MLLMs. By assigning token-rewards to highlight visually critical tokens and incorporating
 118 a fine-grained KL regularization, Cat-PO effectively reduces multimodal hallucinations.
- 119 2. We introduce a hierarchical token-rewards calculation method that relies solely on the
 120 model’s inherent multimodal capabilities, without introducing any external tools or tech-
 121 nologies. Specifically, it first computes global relevance based on cross-modal attention
 122 between text and image, then calculates local relevance based on patch entropy, and finally
 123 uses cross-modal semantic similarity for further refinement.
- 124 3. We conducted extensive experiments across multiple datasets and benchmarks to evaluate
 125 the effectiveness of Cat-PO. Notably, on the AMBER-Generation and MM-Hal benchmarks,
 126 our proposed Cat-PO outperforms existing state-of-the-art methods by 7% – 15% metrics.

128 2 RELATED WORKS

130 2.1 MLLMs HALLUCINATION

132 MLLMs hallucination refers to outputs that are factually inconsistent with the input image, such
 133 as identifying non-existent objects, misdescribing attributes, or misinterpreting relationships. For
 134 example, mentioning a “dog” in a landscape image that contains no animals Bai et al. (2024).

135 To address hallucinations in MLLMs, researchers have proposed a variety of strategies, which broadly
 136 classified as training-free or training-based Xiao et al. (2025). Training-free methods, including
 137 decoding strategies like Opera Huang et al. (2024) and VCD Leng et al. (2024). Training-based
 138 approaches reduce hallucinations through further training. Among these, preference learning such as
 139 RLHF Christiano et al. (2017) are prominent for their efficiency and effectiveness.

141 2.2 PREFERENCE LEARNING FOR HALLUCINATION

142 Preference learning was initially applied to LLM alignment via methods such as RLHF with PPO.
 143 These approaches typically necessitate an explicit reward model and involve complex reinforcement
 144 learning. Recently, DPO has gained widespread adoption as a simpler and more stable alternative to
 145 traditional alignment techniques. HA-DPO Zhao et al. (2023) constructs high-quality sample pairs
 146 for preference learning. Povid Zhou et al. (2024a) creates a fine-grained DPO dataset by injecting
 147 hallucinated text and adding noise to images. MDPO Wang et al. (2024) addresses “unconditional
 148 preference,” where the model may ignore image. CSR Zhou et al. (2024b) iteratively constructs a
 149 preference dataset by self-generating responses, integrating visual constraints into reward modeling.

151 3 METHODOLOGY

153 The overview of our proposed Cat-PO is illustrated in Fig. 2. We first introduce traditional DPO
 154 in Sec. 3.1. Then, we introduce the Hierarchical Visual Relevance of Tokens in Sec. 3.2 and
 155 Token-rewards in Sec. 3.3. Lastly, we describe our novel Cat-PO Loss in Sec. 3.3.

157 3.1 PRELIMINARIES: DIRECT PREFERENCE OPTIMIZATIN (DPO)

159 DPO directly optimizes the model through a contrastive learning objective, making it more inclined
 160 to generate human-preferred responses while reducing the probability of generating dispreferred
 161 responses. DPO learns from preference data $(x, y^+, y^-) \sim \mathcal{D}$, where x is the input prompt, y^+ is the
 human-preferred /chosen response, y^- is the dispreferred /rejected response, and \mathcal{D} is the dataset.

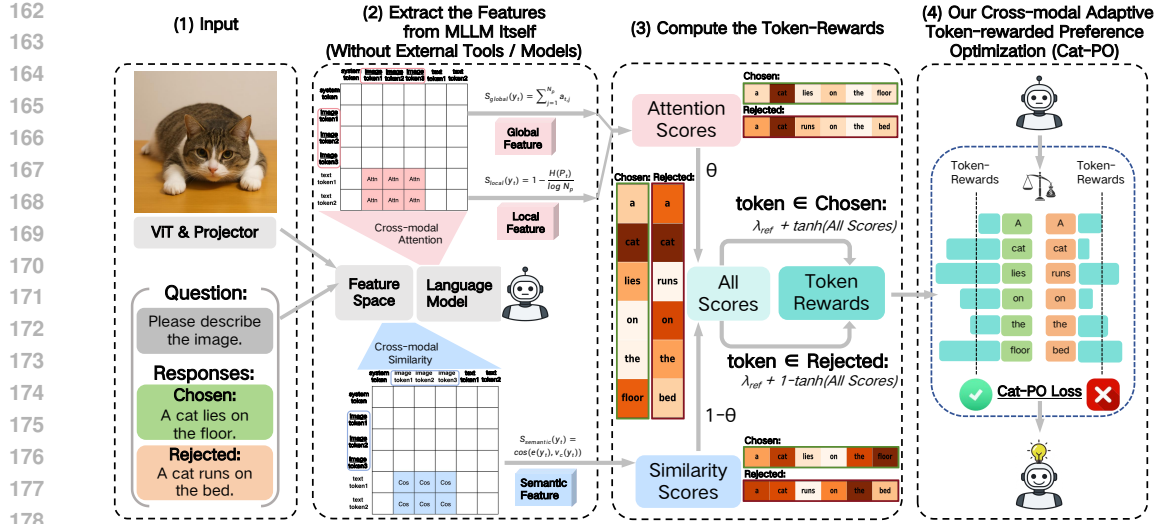


Figure 2: Overview of our proposed Cat-PO framework: (1) The visual images are first projected into the feature space via CLIP+ViT, and the textual question/response tokens are embedded by LLM tokenizer. (2) Cross-modal attention and semantic similarity are extracted in the multi-modal transformer to hierarchically form the global, local, and semantic relevance scores. (3) Token weights are computed by normalizing these scores with positive/negative sample formulas. (4) The weights are integrated into the standard DPO loss to enhance alignment and mitigate hallucinations.

The DPO objective function originates from Bradley-Terry model, which assume that the human preference probability $p^*(y^+ \succ y^- | x)$ can be modeled via a latent reward function $r^*(x, y)$: $p^*(y^+ \succ y^- | x) = \sigma(r^*(x, y^+) - r^*(x, y^-))$. DPO further relates the reward function to the model’s policy π_θ and a reference policy π_{ref} : $r^*(x, y) = \beta(\log(\pi_\theta(y | x)) - \log(\pi_{\text{ref}}(y | x)))$.

where β is a hyperparameter controlling the ratio between reward function and policy deviation. DPO’s loss can directly optimize the model to maximize the probability of generating y^+ and minimize generating y^- . For a given preference pair (x, y^+, y^-) , DPO loss function is defined as:

$$\mathcal{L}_{\text{DPO}} = -\log \sigma \left(\beta \left(\log \frac{\pi_\theta(y^+ | x)}{\pi_{\text{ref}}(y^+ | x)} - \log \frac{\pi_\theta(y^- | x)}{\pi_{\text{ref}}(y^- | x)} \right) \right) \quad (1)$$

By minimizing this loss function, the model π_θ is trained to increase the difference between the log-probabilities of preferred and dispreferred responses, relative to the reference model π_{ref} . This direct method makes DPO simpler and demonstrates comparable or superior performance to RLHF.

3.2 HIERARCHICAL VISUAL RELEVANCE OF TOKENS

Without any external tools or techniques, we leverage the intrinsic multimodal capabilities of MLLMs, to hierarchically compute each token’s global, local, and semantic relevance to the visual input.

3.2.1 CROSS-MODAL ATTENTION BASED GLOBAL RELEVANCE

When MLLMs process DPO training data within the Transformer architectures, the feature representation of each token in a response interacts with visual features via a cross-modal attention mechanism. The activation distribution of these attention scores intuitively reflects the focus of specific text tokens on different image regions. Leveraging this, we define and compute a global relevance score for each token concerning the visual content, thereby quantifying its overall association with the image.

Specifically, for a given image I and its corresponding preferred response y_w or rejected response y_l (collectively denoted y) from the dataset, the representation of the t -th token y_t in y serves as the query. The set of N_p visual token features, $\{v_1, v_2, \dots, v_{N_p}\}$, derived from image I via a visual encoder, acts as the keys and values. The sequence of cross-modal attention scores from token y_t to all N_p visual tokens is denoted by $\{a_{t,1}, a_{t,2}, \dots, a_{t,N_p}\}$.

216 The global relevance $S_{\text{global}}(y_t)$ is defined as the sum of the attention scores for token y_t :
 217

$$218 \quad S_{\text{global}}(y_t) = \sum_{j=1}^{N_p} a_{t,j} \quad (2)$$

219 A higher $S_{\text{global}}(y_t)$ indicates that the model attends more intensively to the entire image when
 220 processing token y_t , implying a stronger global alignment between the token and the visual content.
 221

223 3.2.2 PATCH ENTROPY BASED LOCAL RELEVANCE

225 Although the global relevance score $S_{\text{global}}(y_t)$ captures the overall association between response
 226 tokens and visual content, it does not reveal whether attention is concentrated on key regions or
 227 dispersed across the image. Typically, focused attention indicates a strong link to specific local
 228 information, while dispersed attention suggests higher uncertainty or weaker visual grounding.

229 To accurately characterize the focusing pattern within this attention distribution, we leverage the con-
 230 cept of information entropy to compute the **patch entropy scores** for each token y_t based on its image
 231 attention distribution. First, we extract the cross-modal attention vector $a_t = [a_{t,1}, a_{t,2}, \dots, a_{t,N_p}]$
 232 for token y_t with respect to all N_p image patches, where $a_{t,j}$ represents the attention strength of y_t
 233 towards the j -th image patch. Next, we normalize the attention strengths in a_t to form a probability
 234 distribution $P_t = [P_{t,1}, P_{t,2}, \dots, P_{t,N_p}]$, and $P_{t,j} = a_{t,j} / \sum_{k=1}^{N_p} a_{t,k}$. We then compute the patch
 235 entropy $H(P_t)$ of this probability distribution. To ensure numerical stability in the logarithm, a small
 236 epsilon value ϵ (e.g., 10^{-12}) is introduced:

$$237 \quad H(P_t) = - \sum_{j=1}^{N_p} P_{t,j} \log(P_{t,j} + \epsilon) \quad (3)$$

240 This entropy value $H(P_t)$ measures the uncertainty or dispersion of the attention distribution. Sub-
 241 sequentially, for $N_p > 1$, we normalize the computed entropy $H(P_t)$, and the Patch Entropy Score,
 242 $S_{\text{entropy}}(y_t)$, is then defined as 1 minus this normalized entropy:

$$243 \quad S_{\text{local}}(y_t) = 1 - \frac{H(P_t)}{\log N_p} \quad (\text{for } N_p > 1) \quad (4)$$

244 A higher $S_{\text{local}}(y_t)$ score indicates lower entropy in the attention distribution, implying that attention
 245 is more sharply focused on a few image patches. This generally signifies a stronger degree of
 246 association between the token y_t and specific local regions of the image.

249 3.2.3 CROSS-MODAL SIMILARITY BASED SEMANTIC RELEVANCE

251 Beyond the global and local relevance, we exploit a prior semantic signal obtained from a pretrained
 252 cross-modal encoder to quantify the semantic alignment between response tokens and visual content.

253 Given a sample (I, y) , let the embedding of the t -th token be $\mathbf{e}(y_t)$. The image I is divided into N_p
 254 patches, each encoded as a visual feature $\{\mathbf{v}_1, \dots, \mathbf{v}_{N_p}\}$. With the cross-modal attention weights
 255 $\alpha_{t,j}$ (normalized over patches), we obtain a context-aware visual vector: $\mathbf{v}_c(y_t) = \sum_{j=1}^{N_p} \alpha_{t,j} \mathbf{v}_j$
 256 The semantic relevance score is then defined as

$$258 \quad S_{\text{semantic}}(y_t) = \cos(\mathbf{e}(y_t), \mathbf{v}_c(y_t)) = \frac{\mathbf{e}(y_t) \cdot \mathbf{v}_c(y_t)}{\|\mathbf{e}(y_t)\| \|\mathbf{v}_c(y_t)\|}. \quad (5)$$

261 This score captures the semantic relevance between the token representation and the visual content of
 262 its most attended region, complementing the attention-based global and local relevance.

264 3.3 TOKEN WEIGHTING SCHEME

266 **Unified Visual Relevance Score:** After obtaining hierarchical visual relevance scores for every
 267 response token token y_i , we fuse them into a unified visual relevance score.

$$268 \quad s_i = \alpha [0.5 * S_{\text{global},i} + 0.5 * S_{\text{local},i}] + (1 - \alpha) S_{\text{semantic},i}, \quad \alpha, \mu \in [0, 1]. \quad (6)$$

269 Here, α balances the attention branch (global & local) against the semantic branch.

270 **Smooth Mapping to Token Weights:** Directly injecting s_i into the loss may yield unstable gradients.
 271 We therefore apply a smooth non-linearity: $T_i = \tanh(s_i) \in (0, 1)$, and introduce a base weight
 272 $\lambda_{\text{ref}} > 0$ to maintain a controlled dynamic range:

$$273 \quad 274 \quad 275 \quad w_i = \begin{cases} \lambda_{\text{ref}} + T_i, & y_i \in y^+, \\ \lambda_{\text{ref}} + (1 - T_i), & y_i \in y^-. \end{cases} \quad (7)$$

276 This design (i) rewards tokens in the preferred response that strongly align with the image ($T_i \uparrow$), and
 277 (ii) penalises hallucinated or weakly aligned tokens in the dispreferred response ($(1 - T_i) \uparrow$).
 278

279 3.4 WEIGHTED INTEGRATION AND KL-REGULARISED CAT-PO LOSS

280 Incorporating token weights $\{w_t^+, w_t^-\}$ and token-level KL into the DPO loss yields the Cat-PO loss.
 282

283 **Weighted DPO.** For a preference pair (y^+, y^-) , we weight the log-likelihood ratio of the policy π_θ
 284 and the reference π_{ref} . The weighted policy $\pi_\theta^{(w)}$ is defined as $\pi_\theta^{(w)} = \sum_t (w_t^+ \log \pi_\theta(y_t^+ | h_t^+) -$
 285 $w_t^- \log \pi_\theta(y_t^- | h_t^-))$, and the weighted reference $\pi_{\text{ref}}^{(w)}$ is defined as $\pi_{\text{ref}}^{(w)} = \sum_t (w_t^+ \log \pi_{\text{ref}}(y_t^+ |$
 286 $h_t^+) - w_t^- \log \pi_{\text{ref}}(y_t^- | h_t^-))$. Thus, the weighted DPO loss is defined as:
 287

$$288 \quad \mathcal{L}_{\text{wDPO}} = -\log \sigma[\beta(\pi_\theta^{(w)} - \pi_{\text{ref}}^{(w)})] \quad (8)$$

289 **Token-weighted KL regulariser.** To keep the policy close to the reference and to stabilise training,
 290 with a regularisation strength $\lambda > 0$, we add a token-level, weight-modulated KL penalty:
 291

$$292 \quad 293 \quad \mathcal{L}_{\text{KL}} = \lambda \left(\sum_t w_t^+ \text{KL}[\pi_\theta(\cdot | h_t^+) \| \pi_{\text{ref}}(\cdot | h_t^+)] + \sum_t w_t^- \text{KL}[\pi_\theta(\cdot | h_t^-) \| \pi_{\text{ref}}(\cdot | h_t^-)] \right), \quad (9)$$

294 The final **Cat-PO Loss objective** is:

$$295 \quad 296 \quad \mathcal{L}_{\text{Cat-PO}} = \mathcal{L}_{\text{wDPO}} + \mathcal{L}_{\text{KL}} \quad (10)$$

297 Minimising equation 10 enables the policy model encode human preferences and fine-
 298 grained token–vision alignments, suppressing hallucinations while preserving generation quality.
 299

300 4 EXPERIMENTS

303 4.1 DATASETS AND METRICS

304 **Training Data:** Our experiments primarily employ the widely used RLHF-V dataset Yu et al. (2024).
 305 It comprises 5,733 samples, each including an image, a question, a high-quality response, and a
 306 relatively low-quality response. We use these data to compute token-weights and train our model.
 307

308 **Evaluation Benchmarks:** To comprehensively evaluate the model’s performance in reducing hallu-
 309 cinations and enhancing general capabilities, we employ several widely used benchmarks:

310 For hallucination evaluation, **AMBER** Wang et al. (2023) is a LLM-free benchmark which consists
 311 of two main sub-tasks: (a) *Discrimination*: Determining whether a given statement about an image
 312 is correct or not. (b) *Generation*: Generating a descriptive text based on the image and question.
 313 **MM-Hal** Sun et al. (2023) evaluates response-level hallucination rate and informativeness. It requires
 314 GPT-4 to compare model outputs with human responses and object labels for evaluation.

315 For general capability evaluation, **LLaVA-Bench** Liu et al. (2023b) is a comprehensive benchmark
 316 that uses GPT-4 scoring to evaluate model generalization. **SEED-Bench** Li et al. (2023a) is a
 317 large-scale multimodal benchmark assessing visual understanding and text/image generation.
 318

319 4.2 IMPLEMENTATION DETAILS

321 In our experiments, we leverage the widely adopted LLaVA-v1.5 Liu et al. (2023a) and Qwen2.5-
 322 VL Bai et al. (2025) series models to evaluate the scalability and effectiveness. The training of main
 323 experiment was performed over 6 epochs with an effective batch size of 32, implemented through
 gradient accumulation. And the DPO hyperparameter β_{DPO} set to 0.1.

324 Table 1: Performance comparison on the Discrimination and Generative of AMBER Wang et al.
325 (2023), MM-Hal Sun et al. (2023), LLaVA-Bench Liu et al. (2023b) and SEED Li et al. (2023a)
326 benchmarks. All methods are based on LLaVA-v1.5-7B and -13B Liu et al. (2023b) models with the
327 RLHF-V Yu et al. (2024) dataset, with the best results highlighted in **bold**.

| Method | AMBER-Disc | | AMBER-Gene | | | MM-Hal | | LLaVA ↑ | SEED ↑ |
|-------------------------------|-------------|--------------|------------|-------------|------------|-------------|-------------|-------------|-------------|
| | Acc ↑ | F1 ↑ | CHAIR ↓ | Hal ↓ | Cog ↓ | Score ↑ | Rate ↓ | | |
| LLaVA-v1.5-7B | 71.7 | 74.3 | 7.8 | 36.4 | 4.2 | 2.01 | 61.4 | 65.6 | 66.1 |
| + DPO Rafailov et al. (2023) | 77.5 | 82.1 | 5.7 | 27.3 | 2.6 | 2.14 | 58.3 | 69.1 | 66.4 |
| + CSR Zhou et al. (2024b) | 73.2 | 76.1 | 5.4 | 25.5 | 2.6 | 2.05 | 60.4 | 68.9 | 65.9 |
| + Povid Zhou et al. (2024a) | 71.9 | 74.7 | 5.7 | 26.9 | 3.0 | 2.26 | 55.2 | 68.2 | 66.1 |
| + RLHF-V Yu et al. (2024) | 74.8 | 78.5 | 5.5 | 26.3 | 2.5 | 2.02 | 60.4 | 68.0 | 66.1 |
| + V-DPO Xie et al. (2024) | - | 81.6 | 5.6 | 27.3 | 2.7 | 2.16 | 56.0 | - | - |
| + TPO Gu et al. (2024) | 79.3 | 85.0 | - | - | - | 2.47 | 51.0 | 70.2 | 66.6 |
| + Cat-PO (Ours) | 78.0 | 85.3 | 4.8 | 23.7 | 2.1 | 2.74 | 42.0 | 70.3 | 67.0 |
| LLaVA-v1.5-13B | 71.3 | 73.1 | 7.0 | 33.1 | 3.3 | 2.38 | 53.13 | 73.1 | 68.2 |
| + DPO (Rafailov et al., 2023) | 77.5 | 82.1 | 6.1 | 26.3 | 2.7 | 2.47 | 51.04 | 72.8 | 68.6 |
| + TPO (Gu et al., 2024) | 83.9 | 88.0 | - | - | - | 2.72 | 45.83 | 72.8 | 68.7 |
| + Cat-PO (Ours) | 82.9 | 88.00 | 4.3 | 22.0 | 1.6 | 2.85 | 42.0 | 74.3 | 69.2 |

4.3 MAIN RESULTS

We compare Cat-PO with advanced preference alignment methods, which include: **DPO** Rafailov et al. (2023). **CSR**, Zhou et al. (2024b) A calibrated self-rewarding method. **POVID**, Zhou et al. (2024a) A GPT-4V based alignment method. **RLHF-V**, Yu et al. (2024) A method that segments human preference collection. **TPO**, Gu et al. (2024) A DPO variant employing self-calibrated, visually anchored rewards. **V-DPO**, Xie et al. (2024) A vision-guided DPO variant.

In table 1, we evaluate existing methods and Cat-PO across multiple benchmarks. On the AMBER-Generation and MM-Hal, Cat-PO significantly improves response quality while effectively reducing hallucinations. On the AMBER-Discrimination, it achieves competitive performance, highlighting its ability to evaluate image-related statements. Furthermore, on general benchmarks such as LLaVA-Bench and SEED-Bench, Cat-PO also remains outstanding.

To verify the cross-model generalization of Cat-PO, we also conduct experiments on Qwen-2.5VL-3B Bai et al. (2025). As shown in Fig 3, Cat-PO achieves improvements over Qwen and Qwen+DPO on MM-Hal and AMBER benchmarks, demonstrating its strong generalization ability.

4.4 ABLATION STUDY

Modules’ Contribution. To further validate Cat-PO’s effectiveness, we conducted a comprehensive ablation study in Table 2. The results show that cross-modal attention relevance and semantic relevance play critical roles: weighting either alone improves performance, but their combination yields even greater gains. Moreover, removing the KL-based loss optimization causes a performance drop, confirming the necessity of the token-level KL term.

Impact of Weighted-Tokens Proportion. We further investigate how varying the proportion of weighted tokens in the chosen responses affects Cat-PO performance. As shown in Figure 4 (a),

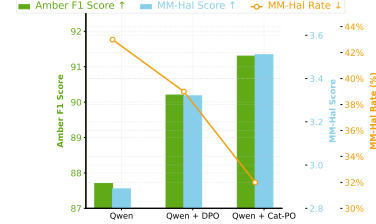


Figure 3: Performance comparison of different Qwen2.5-VL models in terms of AMBER and MM-Hal Benchmarks.

Table 2: Performance of individual Cat-PO modules.

| Modules | MM-Hal | | AMBER-Gene | |
|----------------------|-------------|-------------|------------|-------------|
| | Score ↑ | Rate ↓ | CHAIR ↓ | Hal ↓ |
| DPO-only | 2.14 | 58.3 | 5.7 | 27.3 |
| Attention-only | 2.34 | 55.0 | 5.3 | 25.9 |
| Similarity-only | 2.51 | 47.0 | 5.1 | 27.7 |
| Cat-PO without KL | 2.36 | 53.0 | 5.1 | 26.9 |
| Cat-PO (Ours) | 2.74 | 42.0 | 4.8 | 23.7 |

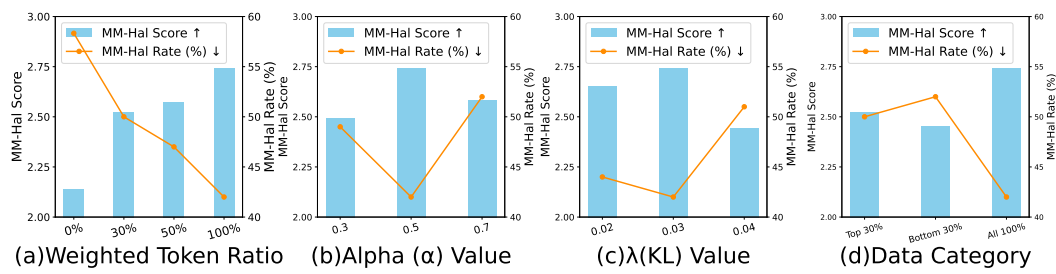


Figure 4: The performance comparison of (a) different weighting proportions, (b)(c) important hyper-parameters α / λ_{KL} , and (d) weighting positions in our proposed Cat-PO framework.

performance steadily improves with increasing weight proportion. However, applying weights to only the top 50% of tokens yields a smaller gain than to the top 30%, indicating that weighting the remaining 50% also provides a notable contribution to overall performance.

Hyperparameter Analysis. We examine two key hyperparameters in Cat-PO: (1) **Balance Coefficient** α . Figure 4 (b) shows that both excessively large and small values of α impair performance, underscoring the need to balance cross-modal attention and semantic relevance; (2) **KL-divergence Coefficient** λ_{KL} . Figure 4 (c) demonstrates that $\lambda_{KL} = 0.03$ achieves the optimal trade-off between maintaining model flexibility and constraining deviation from the reference distribution.

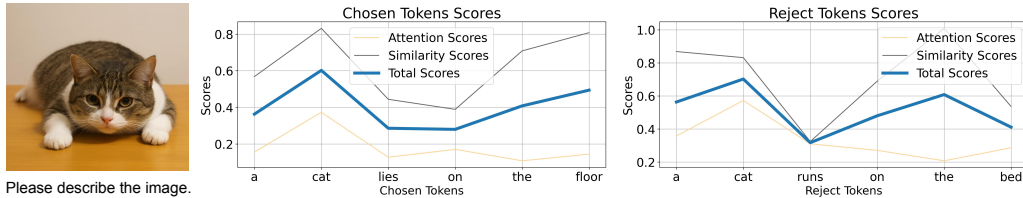


Figure 5: Token-level attention, similarity, and aggregated scores for a single example. The aggregated calculation lifts truly visual tokens (blue) while down-weighting hallucination tokens.

4.5 ANALYSIS EXPERIMENTS

The Effectiveness of Token-Weights Calculation. To further validate the effectiveness of our computed token weights, we applied weighting to either the top 30% or the bottom 30% of tokens. As shown in Figure 4 (d), weighting the top 30% of tokens yields a significant improvement compared to weighting the bottom 30%. This result confirms the accuracy of our weight computation, and demonstrates that key tokens play a decisive role in enhancing the alignment capability.

The Analysis of Training logits. Training logs and visualizations further demonstrate its stability. We track the evolution of the training loss and the reward margin throughout optimization. As shown in Fig. 6, the loss curve decreases smoothly, while the reward margin increases steadily without noticeable oscillations. The monitored gradient norms also remain stable. These observations indicate that Cat-PO maintains good optimization stability under token-level reward modulation.

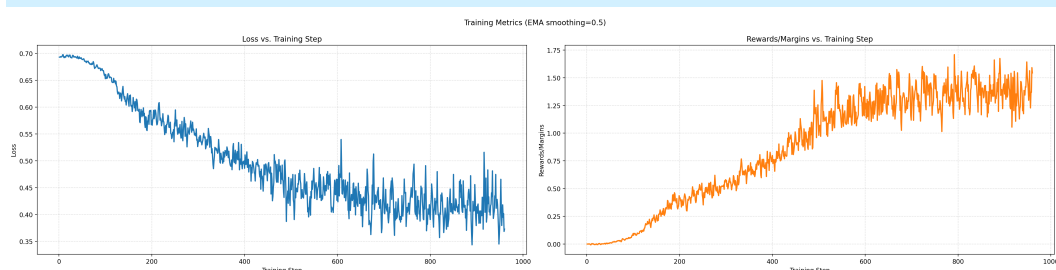


Figure 6: Token-level attention, similarity, and aggregated scores for a single example. The aggregated calculation lifts truly visual tokens (blue) while down-weighting hallucination tokens.

432
433
434
435
436
437
438
439
440
441
442
443
444
445
446
447
448
449
450
451
452
453
454
455
456
457
458
459
460
461
462
463
464
465
466
467
468
469
470
471
472
473
474
475
476
477
478
479
480
481
482
483
484
485

Table 3: CatPO performance on overall and adversarial subsets of POPE Li et al. (2023c).

| CatPO's Score | Acc. | Precision | F1 |
|---------------------------------|------------|------------|------------|
| Average | 85.6 | 95.2 | 84.0 |
| Adversarial (most difficult) | 84.0 (-2%) | 91.3 (-4%) | 82.5 (-2%) |

Table 4: Comparison of Cat-PO (general) and Cat-PO (with learnable fusion).

| Model | MM-Hal (\uparrow) | Hal-Rate (\downarrow) |
|---------------------------------|-----------------------|---------------------------|
| Cat-PO (general) | 2.76 | 49% |
| Cat-PO (w/ learnable fusion) | 2.55 | 50% |

Evaluation on Edge-Case Diagnostics We additionally include POPE benchmark Li et al. (2023c) (with Object, Relation, and Adversarial subset). The Adversarial subset is explicitly designed to elicit visual hallucinations and is widely regarded as the hardest visual alignment benchmark. Table 3 shows that Cat-PO's scores on the adversarial subset are slightly lower than average, indicating that our rewards remain relatively robust even under highly biased and adversarial edge-case settings.

Learnable Fusion Weights. We modified the fusion Eq. 6 to be learnable parameters as follows:

$$s_i = \gamma * S_{\text{global},i} + \delta * S_{\text{local},i} + (1 - \gamma - \delta) * S_{\text{semantic},i}, \quad \gamma, \delta \in [0, 1]. \quad (11)$$

with γ and δ are the learnable parameters. Then, we jointly optimized them within training loss. Table 4 show that introducing learnable coefficients yields the performance below the original one. Learnable fusion showed no benefit, possibly because (1) DPO does not directly supervise weight allocation, causing learnable coefficients to overfit noise, and (2) Cat-PO mainly gains from the complementary cross-modal signals, making the fixed uniform weighting a more stable design.

Robustness Analysis of Token-reward Calculation. To further assess robustness in edge scenarios, we visualize rare cases where attention and similarity disagree (Fig. 7). For “horse”, misaligned attention is corrected by high semantic similarity, while for “train”, an abnormally low similarity score is compensated by sharply focused attention. These examples show that Cat-PO's fused multi-signal scoring mutually compensates single-branch failures instead of amplifying isolated alignment errors.

From a theoretical perspective, Cat-PO computes each token-level reward by fusing three complementary cross-modal signals: global attention, local patch entropy, and cross-modal semantic similarity. A token receives a high reward only when it simultaneously exhibits strong attention strength, a stable focus pattern, and high semantic consistency with visual content. This complementarity reduces reliance on any single noisy branch and structurally limits the misalignment.

Training Overhead Analysis. (1) Only one-time pre-computation: Pre-computing token-level rewards for all positive and negative samples takes 2h16m18s. This cost is incurred only once and the results can be reused indefinitely. (2) We compared the training overhead of Cat-DPO with DPO. Table 5 shows that Cat-PO matches DPO across all metrics, introducing only marginal overhead.

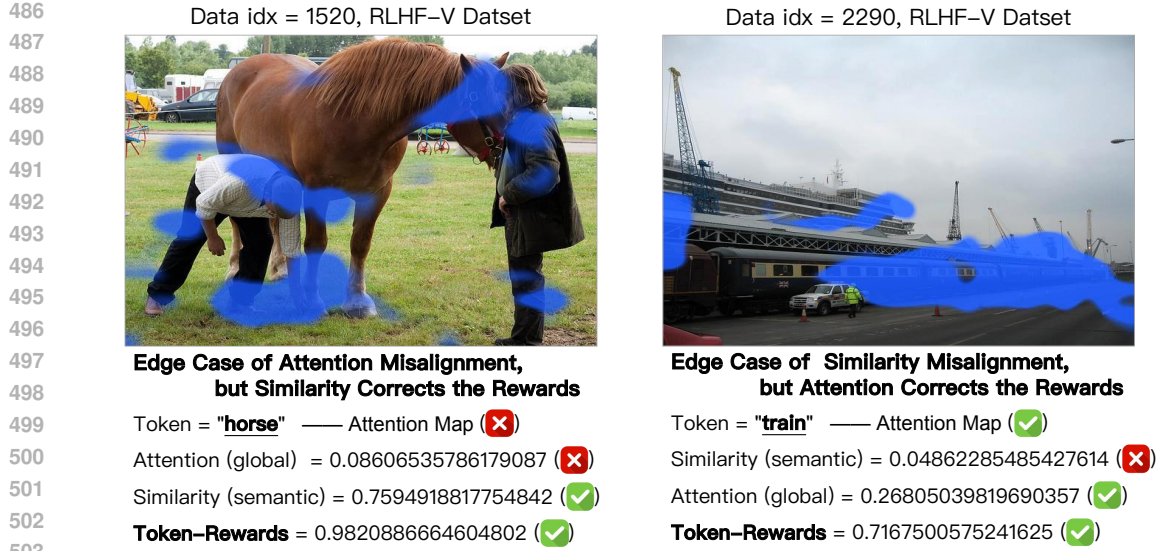
4.6 CASE STUDY

Attention-Similarity Fusion for Token Scoring. Figure 5 illustrates attention scores (global and local), similarity scores, and their weighted sum for a sample. Attention or similarity alone can distinguish visually critical from fact-violating tokens, validating each module's utility. However, biases exist: in the chosen sample, “floor” has a low attention score, while “on” shows low similarity. But fusing the two signals ranks critical tokens higher, enabling precise token weighting in Cat-PO and further supporting our weighting strategy.

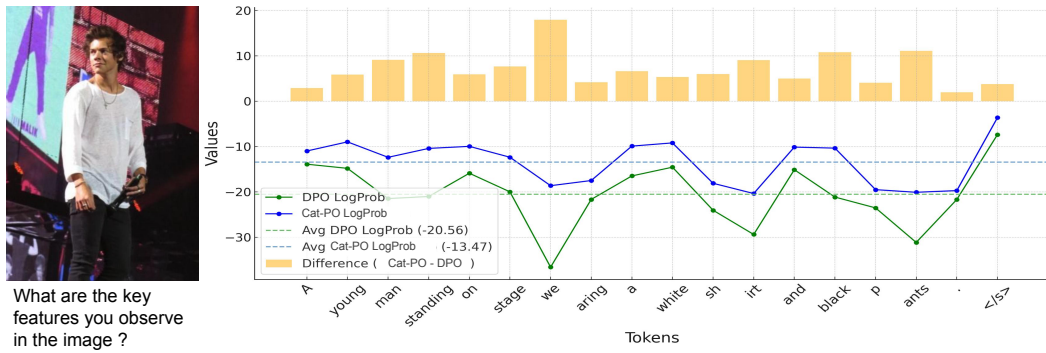
Token-Level Log-Probabilities on Chosen Responses: Cat-PO vs. DPO. To illustrate Cat-PO's advantage in boosting generation confidence, in Figure 8, we present a token-level log-prob case studies. Cat-PO (blue curve) assigns higher log-probabilities to most tokens in chosen responses compared to DPO (green curve), as shown by the consistently positive differences (yellow bars). It

Table 5: Training comparison of DPO vs. Cat-PO: average processing time of per sample and the peak memory usage.

| Model | Avg. time (s) | Peak Memory Usage (GB) |
|---------------|---------------|------------------------|
| DPO | 2.1s | 40.420 |
| Cat-PO (Ours) | 2.9s (+38%) | 40.450 (+0.07%) |



504 Figure 7: Robustness Analysis in Corner Cases of Token-Reward Computation. Blue highlights
 505 indicate regions of concentrated attention. All the data are from RLHF-V Dataset Yu et al. (2024).
 506 Left Part: When visual attention for the token "horse" is misaligned (rarely distributed in horses),
 507 the high semantic similarity effectively rectifies the final reward. Right Part: Conversely, when
 508 the semantic similarity for "train" is anomalously low, the focused attention distribution (correctly
 509 distributed in train) ensures a reasonable reward. This demonstrates that the fused metrics in Cat-PO
 510 mutually compensate for single-metric misalignments, ensuring reliable preference optimization.



524 Figure 8: Log-Probability (log-prob) comparison between Cat-PO and DPO on chosen responses. The
 525 blue (Cat-PO) and green curve (DPO) represent the log-prob. The yellow bars represent differences,
 526 computed as Cat-PO minus DPO. This indicates that Cat-PO not only learns a stronger preference for
 527 chosen responses but also generates them with greater confidence.

528 suggests that Cat-PO better identifies and reinforces key semantic tokens, producing answers that are
 529 both accurate and confidently grounded. Additional cases are provided in Appendix A.4.

530 **Comparison of Cat-PO and DPO Generations.** The comparison is presented in Appendix A.5.

5 CONCLUSION

536 In this paper, we propose Cross-modal Adaptive Token-rewarded Preference Optimization (Cat-PO)
 537 for mitigating hallucinations and improving MLLM truthfulness. Each token's global, local, and
 538 semantic relevance is computed from cross-modal attention and similarity, fused and incorporated
 539 into the DPO loss for fine-grained optimization. Experiments on public benchmarks show that Cat-PO
 effectively reduces hallucinations, improves response accuracy, enhances MLLMs truthfulness.

540 REFERENCES
541

542 Elmira Amirloo, Jean-Philippe Fauconnier, Christoph Roesmann, Christian Kerl, Rinu Boney, Yusu
543 Qian, Zirui Wang, Afshin Dehghan, Yinfei Yang, Zhe Gan, et al. Understanding alignment in
544 multimodal llms: A comprehensive study. *arXiv preprint arXiv:2407.02477*, 2024.

545 Shuai Bai, Keqin Chen, Xuejing Liu, Jialin Wang, Wenbin Ge, Sibo Song, Kai Dang, Peng Wang,
546 Shijie Wang, Jun Tang, Humen Zhong, Yuanzhi Zhu, Mingkun Yang, Zhaohai Li, Jianqiang Wan,
547 Pengfei Wang, Wei Ding, Zheren Fu, Yiheng Xu, Jiabo Ye, Xi Zhang, Tianbao Xie, Zesen Cheng,
548 Hang Zhang, Zhibo Yang, Haiyang Xu, and Junyang Lin. Qwen2.5-vl technical report. *arXiv*
549 *preprint arXiv:2502.13923*, 2025.

550 Zechen Bai, Pichao Wang, Tianjun Xiao, Tong He, Zongbo Han, Zheng Zhang, and Mike Zheng Shou.
551 Hallucination of multimodal large language models: A survey. *arXiv preprint arXiv:2404.18930*,
552 2024.

553 Assaf Ben-Kish, Moran Yanuka, Morris Alper, Raja Giryes, and Hadar Averbuch-Elor. Mocha:
554 Multi-objective reinforcement mitigating caption hallucinations. *arXiv preprint arXiv:2312.03631*,
555 2, 2023.

556 Yangyi Chen, Karan Sikka, Michael Cogswell, Heng Ji, and Ajay Divakaran. Dress: Instructing
557 large vision-language models to align and interact with humans via natural language feedback.
558 In *Proceedings of the IEEE/CVF Conference on Computer Vision and Pattern Recognition*, pp.
559 14239–14250, 2024.

560 Paul F Christiano, Jan Leike, Tom Brown, Miljan Martic, Shane Legg, and Dario Amodei. Deep
561 reinforcement learning from human preferences. *Advances in neural information processing*
562 systems, 30, 2017.

563 Jinlan Fu, Shenzhen Huangfu, Hao Fei, Xiaoyu Shen, Bryan Hooi, Xipeng Qiu, and See-Kiong Ng.
564 Chip: Cross-modal hierarchical direct preference optimization for multimodal llms. *arXiv preprint*
565 *arXiv:2501.16629*, 2025.

566 Jihao Gu, Yingyao Wang, Meng Cao, Pi Bu, Jun Song, Yancheng He, Shilong Li, and Bo Zheng.
567 Token preference optimization with self-calibrated visual-anchored rewards for hallucination
568 mitigation. *arXiv preprint arXiv:2412.14487*, 2024.

569 Tianrui Guan, Fuxiao Liu, Xiyang Wu, Ruiqi Xian, Zongxia Li, Xiaoyu Liu, Xijun Wang, Lichang
570 Chen, Furong Huang, Yaser Yacoob, et al. Hallusionbench: an advanced diagnostic suite for entan-
571 gled language hallucination and visual illusion in large vision-language models. In *Proceedings of*
572 *the IEEE/CVF Conference on Computer Vision and Pattern Recognition*, pp. 14375–14385, 2024.

573 Anisha Gunjal, Jihan Yin, and Erhan Bas. Detecting and preventing hallucinations in large vision
574 language models. In *Proceedings of the AAAI Conference on Artificial Intelligence*, volume 38, pp.
575 18135–18143, 2024.

576 Qidong Huang, Xiaoyi Dong, Pan Zhang, Bin Wang, Conghui He, Jiaqi Wang, Dahua Lin, Weiming
577 Zhang, and Nenghai Yu. Opera: Alleviating hallucination in multi-modal large language models
578 via over-trust penalty and retrospection-allocation. In *Proceedings of the IEEE/CVF Conference*
579 *on Computer Vision and Pattern Recognition*, pp. 13418–13427, 2024.

580 Sicong Leng, Hang Zhang, Guanzheng Chen, Xin Li, Shijian Lu, Chunyan Miao, and Lidong Bing.
581 Mitigating object hallucinations in large vision-language models through visual contrastive decod-
582 ing. In *Proceedings of the IEEE/CVF Conference on Computer Vision and Pattern Recognition*,
583 pp. 13872–13882, 2024.

584 Bohao Li, Rui Wang, Guangzhi Wang, Yuying Ge, Yixiao Ge, and Ying Shan. Seed-bench: Bench-
585 marking multimodal llms with generative comprehension. *arXiv preprint arXiv:2307.16125*,
586 2023a.

587 Lei Li, Zhihui Xie, Mukai Li, Shunian Chen, Peiyi Wang, Liang Chen, Yazheng Yang, Benyou
588 Wang, and Lingpeng Kong. Silkie: Preference distillation for large visual language models. *arXiv*
589 *preprint arXiv:2312.10665*, 2023b.

594 Yifan Li, Yifan Du, Kun Zhou, Jinpeng Wang, Wayne Xin Zhao, and Ji-Rong Wen. Evaluating object
 595 hallucination in large vision-language models. *arXiv preprint arXiv:2305.10355*, 2023c.
 596

597 Zijing Liang, Yanjie Xu, Yifan Hong, Penghui Shang, Qi Wang, Qiang Fu, and Ke Liu. A survey
 598 of multimodel large language models. In *Proceedings of the 3rd International Conference on*
 599 *Computer, Artificial Intelligence and Control Engineering*, pp. 405–409, 2024.

600 Hanchao Liu, Wenyuan Xue, Yifei Chen, Dapeng Chen, Xiutian Zhao, Ke Wang, Liping Hou,
 601 Rongjun Li, and Wei Peng. A survey on hallucination in large vision-language models. *arXiv*
 602 *preprint arXiv:2402.00253*, 2024a.
 603

604 Haotian Liu, Chunyuan Li, Qingyang Wu, and Yong Jae Lee. Visual instruction tuning, 2023a.
 605

606 Haotian Liu, Chunyuan Li, Qingyang Wu, and Yong Jae Lee. Visual instruction tuning. *Advances in*
 607 *neural information processing systems*, 36:34892–34916, 2023b.
 608

609 Haotian Liu, Chunyuan Li, Yuheng Li, and Yong Jae Lee. Improved baselines with visual instruction
 610 tuning. In *Proceedings of the IEEE/CVF Conference on Computer Vision and Pattern Recognition*,
 611 pp. 26296–26306, 2024b.
 612

613 Renjie Pi, Tianyang Han, Wei Xiong, Jipeng Zhang, Runtao Liu, Rui Pan, and Tong Zhang. Strengthening
 614 multimodal large language model with bootstrapped preference optimization. In *European*
 615 *Conference on Computer Vision*, pp. 382–398. Springer, 2024.
 616

617 Alec Radford, Jong Wook Kim, Chris Hallacy, Aditya Ramesh, Gabriel Goh, Sandhini Agarwal,
 618 Girish Sastry, Amanda Askell, Pamela Mishkin, Jack Clark, et al. Learning transferable visual
 619 models from natural language supervision. In *International conference on machine learning*, pp.
 620 8748–8763. PMLR, 2021.
 621

622 Rafael Rafailov, Archit Sharma, Eric Mitchell, Christopher D Manning, Stefano Ermon, and Chelsea
 623 Finn. Direct preference optimization: Your language model is secretly a reward model. *Advances*
 624 *in Neural Information Processing Systems*, 36:53728–53741, 2023.
 625

626 Zhiqing Sun, Sheng Shen, Shengcao Cao, Haotian Liu, Chunyuan Li, Yikang Shen, Chuang Gan,
 627 Liang-Yan Gui, Yu-Xiong Wang, Yiming Yang, et al. Aligning large multimodal models with
 628 factually augmented rlhf. *arXiv preprint arXiv:2309.14525*, 2023.
 629

630 Fei Wang, Wenzuan Zhou, James Y Huang, Nan Xu, Sheng Zhang, Hoifung Poon, and Muahao Chen.
 631 mdpo: Conditional preference optimization for multimodal large language models. *arXiv preprint*
 632 *arXiv:2406.11839*, 2024.
 633

634 Junyang Wang, Yuhang Wang, Guohai Xu, Jing Zhang, Yukai Gu, Haitao Jia, Ming Yan, Ji Zhang,
 635 and Jitao Sang. An llm-free multi-dimensional benchmark for mllms hallucination evaluation.
 636 *arXiv preprint arXiv:2311.07397*, 2023.
 637

638 Wenyi Xiao, Ziwei Huang, Leilei Gan, Wanggui He, Haoyuan Li, Zhelun Yu, Fangxun Shu, Hao
 639 Jiang, and Linchao Zhu. Detecting and mitigating hallucination in large vision language models
 640 via fine-grained ai feedback. *arXiv preprint arXiv:2404.14233*, 2024.
 641

642 Wenyi Xiao, Ziwei Huang, Leilei Gan, Wanggui He, Haoyuan Li, Zhelun Yu, Fangxun Shu, Hao
 643 Jiang, and Linchao Zhu. Detecting and mitigating hallucination in large vision language models
 644 via fine-grained ai feedback. In *Proceedings of the AAAI Conference on Artificial Intelligence*,
 645 volume 39, pp. 25543–25551, 2025.
 646

647 Yuxi Xie, Guanzhen Li, Xiao Xu, and Min-Yen Kan. V-dpo: Mitigating hallucination in
 648 large vision language models via vision-guided direct preference optimization. *arXiv preprint*
 649 *arXiv:2411.02712*, 2024.
 650

651 Tianyu Yu, Yuan Yao, Haoye Zhang, Taiwen He, Yifeng Han, Ganqu Cui, Jinyi Hu, Zhiyuan Liu,
 652 Hai-Tao Zheng, Maosong Sun, et al. Rlhf-v: Towards trustworthy mllms via behavior alignment
 653 from fine-grained correctional human feedback. In *Proceedings of the IEEE/CVF Conference on*
 654 *Computer Vision and Pattern Recognition*, pp. 13807–13816, 2024.
 655

648 Yongcheng Zeng, Guoqing Liu, Weiyu Ma, Ning Yang, Haifeng Zhang, and Jun Wang. Token-level
 649 direct preference optimization. *arXiv preprint arXiv:2404.11999*, 2024.
 650

651 Kejia Zhang, Keda Tao, Zhiming Luo, Chang Liu, Jiasheng Tang, and Huan Wang. Tars: Minmax
 652 token-adaptive preference strategy for hallucination reduction in mllms. *arXiv e-prints*, pp. arXiv-
 653 2507, 2025.

654 Mengxi Zhang, Wenhao Wu, Yu Lu, Yuxin Song, Kang Rong, Huanjin Yao, Jianbo Zhao, Fanglong
 655 Liu, Haocheng Feng, Jingdong Wang, et al. Automated multi-level preference for mllms. *Advances*
 656 *in Neural Information Processing Systems*, 37:26171–26194, 2024.
 657

658 Zhiyuan Zhao, Bin Wang, Linke Ouyang, Xiaoyi Dong, Jiaqi Wang, and Conghui He. Beyond
 659 hallucinations: Enhancing lylms through hallucination-aware direct preference optimization. *arXiv*
 660 *preprint arXiv:2311.16839*, 2023.

661 Yiyang Zhou, Chenhang Cui, Rafael Rafailev, Chelsea Finn, and Huaxiu Yao. Aligning modalities in
 662 vision large language models via preference fine-tuning. *arXiv preprint arXiv:2402.11411*, 2024a.
 663

664 Yiyang Zhou, Zhiyuan Fan, Dongjie Cheng, Sihan Yang, Zhaorun Chen, Chenhang Cui, Xiyao Wang,
 665 Yun Li, Linjun Zhang, and Huaxiu Yao. Calibrated self-rewarding vision language models. *arXiv*
 666 *preprint arXiv:2405.14622*, 2024b.

667 Ke Zhu, Liang Zhao, Zheng Ge, and Xiangyu Zhang. Self-supervised visual preference alignment.
 668 *In Proceedings of the 32nd ACM International Conference on Multimedia*, pp. 291–300, 2024.
 669

670 Mingkang Zhu, Xi Chen, Zhongdao Wang, Bei Yu, Hengshuang Zhao, and Jiaya Jia. Tgdpo:
 671 Harnessing token-level reward guidance for enhancing direct preference optimization. *arXiv*
 672 *preprint arXiv:2506.14574*, 2025.

673

674 A APPENDIX

675 A.1 USAGE OF LARGE LANGUAGE MODELS IN MANUSCRIPT PREPARATION

676 To ensure the clarity, fluency, and grammatical accuracy of the manuscript, large language models
 677 (LLMs) were employed during the preparation process, specifically for two core tasks: text polishing
 678 and grammatical error correction. In terms of text polishing, LLMs were used to optimize the
 679 expression of technical content (including experimental descriptions, result analyses, and discus-
 680 sion sections) — this involved refining sentence structure to enhance logical coherence, adjusting
 681 terminology consistency to align with academic conventions in the field of machine learning (e.g.,
 682 standardizing the naming of "Cat-PO model" and "baseline DPO model" throughout the text), and
 683 improving the readability of complex statistical interpretations . For grammatical error correction,
 684 LLMs assisted in identifying and rectifying potential issues in English expression (including subject-
 685 verb agreement, tense consistency, and preposition usage) to eliminate language-related ambiguities
 686 that might affect the understanding of research findings. It is important to note that all core research
 687 content — including experimental design, data collection, model training processes, statistical analy-
 688 ses, and key conclusions — remained independently completed by the authors, and LLMs were only
 689 used as auxiliary tools for language optimization without altering any substantive research content.
 690

691 A.2 LIMITATIONS AND FUTURE WORK.

692 Our approach relies solely on the intrinsic multi-modal capabilities of MLLMs, without external
 693 tools or models. This work primarily validates effectiveness and provides qualitative analysis. Future
 694 work will systematically measure resource consumption, expand evaluation metrics, and verify the
 695 resource savings from our eliminating external dependencies.

696 A.3 ADDITIONAL RELATED WORKS.

697 **In more fine-grained DPO explorations**, CHiP Fu et al. (2025) introduces visual preference op-
 698 timization together with hierarchical preference optimization at the response, segment, and token

702 levels on the text side. The token-level component is primarily based on sequence-level KL divergence 703 derived from text probability distributions; it is not image-aware and functions only as an 704 auxiliary term in the text-side loss. TARS Zhang et al. (2025) reformulates DPO as a min–max game. 705 TARS introduces adaptive perturbations on vision-irrelevant tokens to induce controlled distribution 706 shifts and combines them with a frequency-domain regularization constraint, achieving substantial 707 improvements in visual grounding and robustness under very low data costs. AMP Zhang et al. (2024) 708 leverages multi-level preferences to construct finer-grained preference orderings, effectively reducing 709 the quality gap between positive and negative samples. It focuses on response-level alignment by 710 incorporating multiple preference levels.

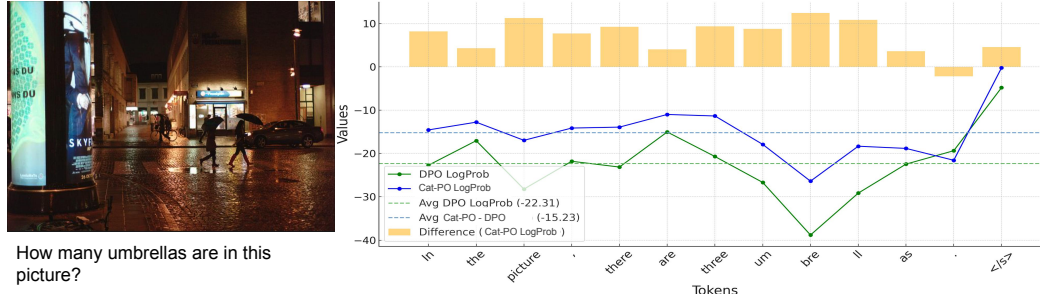
711 **In pure-text LLMs.** TGDPO Zhu et al. (2025) introduces a reward-guided DPO framework that 712 decomposes sequence-level PPO into token-level subproblems and theoretically proves the indepen- 713 dence of the partition function. This enables the integration of fine-grained token-level rewards into 714 the DPO objective, improving instruction-following performance and training stability. TDPO Zeng 715 et al. (2024) further decomposes sentence-level rewards into token-level rewards via the Bellman 716 equation and introduces a Sequential Forward KL constraint. Through token-level optimization, 717 TDPO enhances alignment performance in text-only generation.

718 **Other related works.** Hallucinations in MLLMs from several factors: training data deficiencies Li 719 et al. (2023c); module-specific issues within MLLMs’ separately trained components Guan et al. 720 (2024); suboptimal training paradigms Ben-Kish et al. (2023); and inference-stage defects 721

722 Recently, RLHF-V Yu et al. (2024) collects segment-level human preference data and performs 723 dense DPO training. TPO Gu et al. (2024) explores token-level information in DPO for LVLMs. 724 V-DPO Xie et al. (2024) pairs response preferences with image-contrast preferences and employs 725 vision-guided DPO to reinforce visual context learning.

726 A.4 MORE CASE OF TOKEN-LEVEL LOG-PROBABILITIES ON CHOSEN RESPONSES.

727
728
729 In Figure 9, We have included an additional case study in this subsection. This example provides 730 further evidence regarding the distinct token-level log-probabilities on the chosen responses, demon- 731 strating our method’s robust confidence.



756 Figure 9: Log-Probability (log-prob) comparison between Cat-PO and DPO on chosen responses. The 757 blue (Cat-PO) and green curve (DPO) represent the log-prob. The yellow bars represent differences, 758 computed as Cat-PO minus DPO. This indicates that Cat-PO not only learns a stronger preference for 759 chosen responses but also generates them with greater confidence.

760 A.5 COMPARISON OF GENERATION IN CAT-PO AND DPO.

761 Our comparative analysis (see Figure 10 in Appendix A.5) illustrates the performance differences 762 between Cat-PO and DPO across four distinct examples. The figure contains four sub-examples 763 demonstrating Cat-PO’s consistent advantage in generating more detailed and accurate descriptions, 764 particularly in identifying subject counts, positional relationships, and contextual details.

| | | | | |
|-----|---|---|------------|---|
| 756 | Example1 |  | DPO | The image captures a person, likely a woman, riding a horse on the beach. The rider is wearing a helmet for safety while enjoying the ride. The horse is a gray-colored animal, adding a sense of motion and speed to the scene. The beach setting with the ocean in the background creates a serene and picturesque backdrop for this equestrian activity. |
| 757 | | | Our Cat-PO | The image features a person riding a horse on a beach, with the horse running along the shoreline. The person is wearing a black jacket and a hat, and they are skillfully riding the horse. The horse is positioned towards the center of the image, with the person on its back. The beach setting provides a picturesque and serene atmosphere for the rider and the horse. |
| 758 | | | | |
| 759 | | | | |
| 760 | | | | |
| 761 | | | | |
| 762 | | | | |
| 763 | | | | |
| 764 | | | | |
| 765 | Example2 |  | DPO | The image features a person riding a skateboard on a beach. The skateboarder is the main subject of the scene, as they navigate the sandy terrain while maintaining their balance on the skateboard. The backdrop consists of a sky with clouds, creating a serene and open atmosphere. |
| 766 | | | Our Cat-PO | The image features a man riding a skateboard down a sandy hill, enjoying the thrill of the descent. The skateboarder is positioned in the middle of the scene, with the skateboard visible beneath him. The hill appears to be a sandy dune, and the man seems to be skillfully navigating the terrain. The sky in the background is blue, adding to the overall atmosphere of the scene. |
| 767 | | | | |
| 768 | | | | |
| 769 | | | | |
| 770 | | | | |
| 771 | | | | |
| 772 | | | | |
| 773 | | | | |
| 774 | Example1 |  | DPO | The image features two dogs of different colors walking on a sandy beach. They appear to be enjoying their time outdoors, possibly exploring or taking a stroll along the shore. The beach setting and the presence of the dogs create a sense of leisure and freedom, as they roam freely in this natural environment. |
| 775 | | | Our Cat-PO | The image features a sandy beach with three dogs walking together. The dogs are of different colors, with one being black and white, another brown and white, and the third one being brown. They are walking in a line, with the black and white dog leading the way, followed by the brown and white dog, and then the brown dog. The dogs appear to be enjoying their time on the beach, possibly exploring or playing. |
| 776 | | | | |
| 777 | | | | |
| 778 | | | | |
| 779 | | | | |
| 780 | | | | |
| 781 | | | | |
| 782 | | | | |
| 783 | Example2 |  | DPO | The image features two children, a young boy and a young girl, playing in a grassy field on a sunny day. They appear to be enjoying their time outdoors, possibly exploring or having fun together. The green grass and the sunlight create a pleasant atmosphere for the children to engage in their play activities. |
| 784 | | | Our Cat-PO | The image features a lush green field with three children playing together. Two of the children are standing, while the third child is sitting on the grass. The two standing children are positioned closer to the left side of the image, while the sitting child is on the right side. In the scene, there is a toy visible, likely a toy car, placed near the left side of the image. The children seem to be enjoying their time outdoors, playing and having fun in the grassy field. |
| 785 | | | | |
| 786 | | | | |
| 787 | | | | |
| 788 | | | | |
| 789 | | | | |
| 790 | | | | |
| 791 | | | | |
| 792 | | | | |
| 793 | | | | |
| 794 | Figure 10: Four comparative examples showing generation differences between DPO and our Cat-PO. (1) Beach horse riding: Cat-PO provides specific details about rider attire and horse movement. (2) Sand skateboarding: Cat-PO adds contextual information about terrain and activity. (3) Beach dogs: Cat-PO correctly identifies three dogs with distinct color patterns. (4) Children playing: Cat-PO notes precise subject count, positions, and presence of a toy. | | | |
| 795 | | | | |
| 796 | | | | |
| 797 | | | | |
| 798 | | | | |
| 799 | | | | |
| 800 | | | | |
| 801 | A.6 QUANTITATIVE EVALUATION: SUPERIORITY OF CAT-PO IN BOOSTING TOKEN-LEVEL LOG-PROBABILITIES | | | |
| 802 | | | | |
| 803 | | | | |
| 804 | Our supplementary statistical analysis further quantifies the significant effect of the Cat-PO model in enhancing the generation confidence of positive responses compared to the baseline DPO model. The distributional statistics, illustrated in Figure 11, reveal the widespread positive impact of Cat-PO: on average, a remarkable 97% of tokens within each positive sample experienced a positive increase in their log-probability. Furthermore, at the overall sample level, 99.98% of the samples in the dataset demonstrated a net growth in total log-probability (sum of log-probability improvements across all tokens) under the Cat-PO model. These figures robustly demonstrate that the Cat-PO method is not | | | |
| 805 | | | | |
| 806 | | | | |
| 807 | | | | |
| 808 | | | | |
| 809 | | | | |

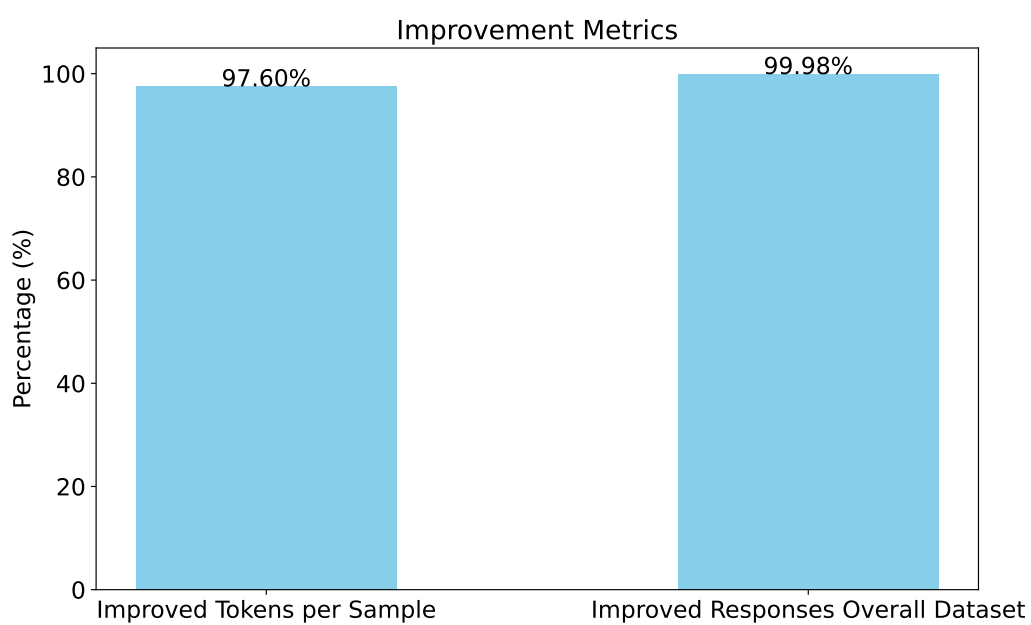


Figure 11: Improvement metrics for the model trained with Cat-PO in enhancing positive sample responses. The left bar indicates that, under the Cat-PO model, an average of 97.60% of tokens within each positive sample response experienced a positive increase in their log-probability. The right bar shows that 99.98% of the samples in the dataset demonstrated a net growth in total log-probability under the Cat-PO model.

only highly effective but also that its advantages are broadly applicable, covering almost all test data and the vast majority of generated content.

Regarding the magnitude of improvement, our statistical results are equally encouraging (this can be linked to your second figure if it shows magnitude, or stated directly). Specifically, the Cat-PO model achieved an average log-probability increase of 7.911821 per token in positive responses. When converted to a relative percentage, the average percentage increase in log-probability per token reached 29.96%. This substantial level of improvement, especially in the log-space, signifies that the Cat-PO model exhibits far greater "certainty" than the baseline model when generating key parts of these preferred responses.